ACS APPLIED MATERIALS & INTERFACES

www.acsami.org

Research Article

Muramyl Dipeptide-Presenting Polymersomes as Artificial Nanobacteria to Boost Systemic Antitumor Immunity

Guanhong Cui, Yinping Sun, Shenqiang Wang, Fenghua Meng, and Zhiyuan Zhong*

Cite This: *ACS Appl. Mater. Interfaces* 2024, 16, 61655−61663

Read Online

ACCESS | Metrics & More | Article Recommendations | Supporting Information

ABSTRACT: The clinical efficacy of cancer vaccines is closely related to immunoadjuvants that play a crucial role in magnifying and prolonging the immune response. Muramyl dipeptide (MDP), a minimal and conserved peptidoglycan found in almost all bacteria, can trigger robust immune activation by uniquely antagonizing the nucleotide-binding oligomerization domain 2 (NOD2) pathway. However, its effectiveness has been hindered by limited solubility, poor membrane penetration, and rapid clearance from the body. Here, we introduce MDP-presenting polymersomes as artificial nanobacteria (NBA) to boost the antitumor immune response. The NBA, featuring abundant MDP molecules, induces superior stimulation of immune cells including macrophages and bone marrow-derived dendritic cells (BMDCs) compared to free MDP, likely via facilitating immune cell uptake and cooperatively stimulating systemic NOD2 signaling. Importantly, systemic administration of NBA significantly enhances the chemo-immunotherapy of B16-F10 melanoma-bearing mice pretreated with doxorubicin by reversing the immunosuppressive tumor microenvironment. Furthermore, NBA carrying ovalbumin and B16-F10 cell lysates induces robust OVA-IgG antibody production and effectively inhibit tumor growth, respectively. The artificial nanobacteria hold great promise as a potent systemic immunoadjuvant for cancer immunotherapy.

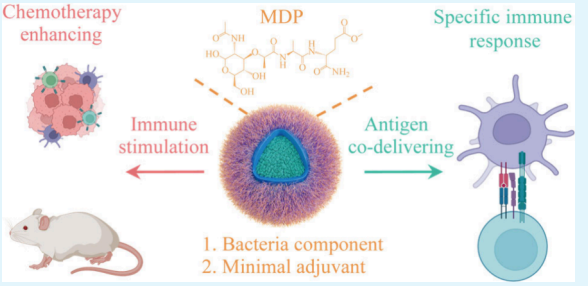

KEYWORDS: *chemo-immunotherapy, immunoadjuvant, tumor microenvironment, polymersomes, cancer vaccines*

1. INTRODUCTION

Cancer vaccines involve utilizing tumor antigens to stimulate the patient's adaptive immune system for immune recognition and elimination of tumor cells, thereby revolutionizing tumor immunotherapy.[1,2] Efficient antigen presentation by antigen-presenting cells (APCs), such as dendritic cells (DCs), to T leukocytes facilitates tumor inhibition.[3] Current approaches focus on vaccine formulation, with an emphasis on codelivering immunoadjuvants to enhance immune responses.[4,5] Various types of immunoadjuvants, including toll-like receptor (TLR) agonists, NOD-like receptor (NLR) agonists, stimulators of the interferon genes (STING) pathway, exosomes, as well as metallic or plant-derived immunoadjuvants, have been confirmed for their immunological effects.[6−10] Despite the significant achievements of immunoadjuvant-assisted cancer vaccines in tumor regression and extended survival, the ongoing challenge of insufficient immunogenicity remains a critical obstacle.[11]

Nucleotide-binding oligomerization domain 2 (NOD2) has the potential to enhance the currently restricted array of vaccine adjuvants, owing to its extensive immunomodulatory effects.[12] Muramyl dipeptide (MDP), a minimal and conserved peptidoglycan found in nearly all bacteria, is recognized as a pathogen-associated molecular pattern (PAMP) that offers distinct advantages as an immunoadjuvant compared to traditional agents.[12,13] For instance, MDP has been shown to possess the capability to stimulate both humoral and cellular immune responses.[14] The recognition of MDP initiates downstream signaling cascades, such as the mitogen-activated protein kinase (MAPK), AP-1, and nuclear factor κB (NF-κB) pathways, through self-oligomerization mediated by NOD2, resulting in a pathogen recognition and immune response.[15−17] Furthermore, MDP has demonstrated effectiveness as an immunoadjuvant for chemotherapy.[18−20] Nevertheless, clinical utilization of MDP has been hindered by challenges including limited solubility, poor membrane penetration, and rapid clearance from the body.[21] Enhancing the lipophilicity of MDP presents a promising strategy to augment its pharmacological properties.[22] Liposomes, as highly effective lipophilic drug carriers, can enhance drug bioavailability by incorporating lipophilic MDP analogs into their lipid bilayers to facilitate targeted drug delivery.[23−25] However, the rapid clearance of liposomal MDP formulations from circulation remains a

Received: August 2, 2024
Revised: October 15, 2024
Accepted: October 27, 2024
Published: November 5, 2024

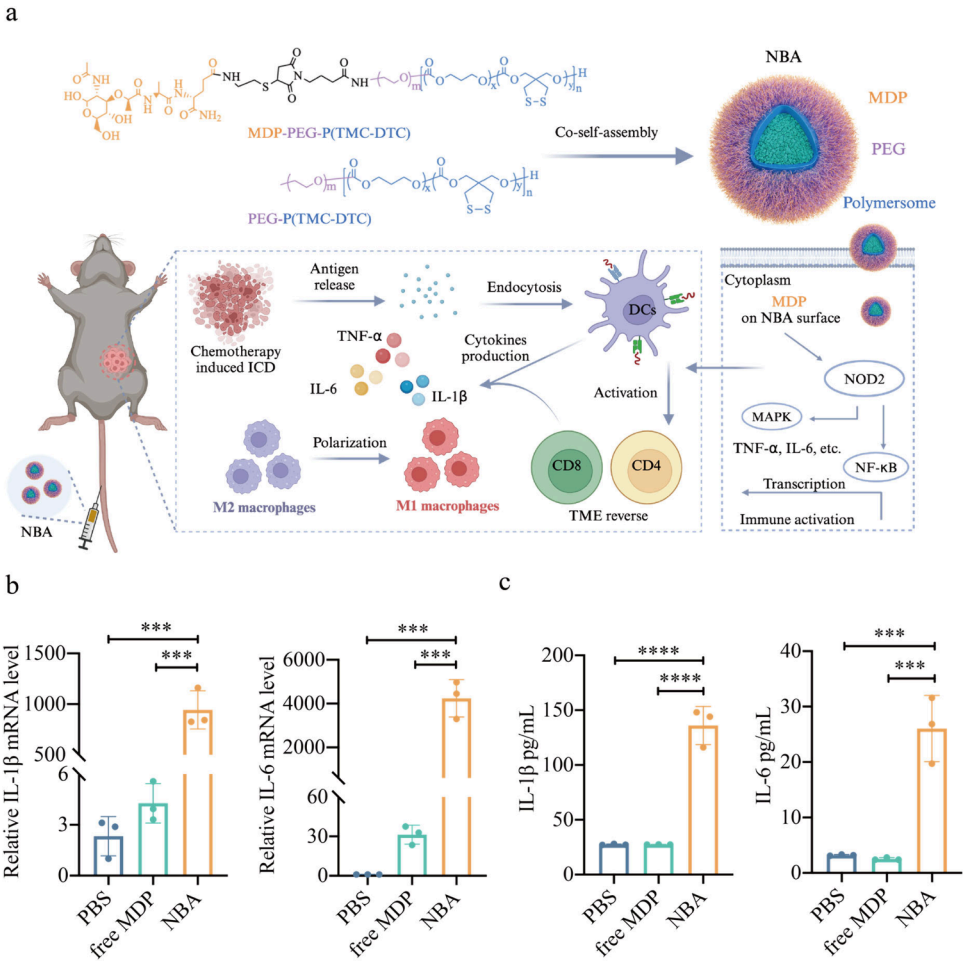

Figure 1. Preparation of nanobacteria (NBA) and activation of macrophage inflammatory signaling pathway by NBA *in vitro*. (a) Schematic illustration of the construction of NBA for enhancing chemo-immunotherapeutic efficiency. Mice receiving chemotherapy caused tumor immunogenic cell death (ICD) and released tumor antigens. After systemic injection, NBA could promote the maturation and antigen presentation of DC cells for activating the tumor-infiltrating T-cells, while NBA repolarized M2 macrophages to M1 macrophages. Ultimately, NBA improved the efficacy of chemotherapy and reversed the tumor microenvironment (TME). (b, c) NBA induced the proinflammatory signals upregulation in RAW 264.7 macrophages ($n = 3$). (b) The mRNA expression levels of IL-1β and IL-6 were analyzed by RT-PCR ($n = 3$), and (c) the secreted cytokines in the supernatant were analyzed by ELISA; p value: ***$p < 0.001$; ****$p < 0.0001$.

significant hurdle, with only a minute fraction of the administered dosage persisting in the plasma after 5 min.[26] Potential drug leakage during circulation due to liposome instability further exacerbates this challenge.[27,28] Consequently, the development of well-defined MDP delivery platforms with enhanced structural stability for cancer vaccination aimed at eliciting a controlled, yet potent, tumor-specific T-cell response represents a pivotal area for further exploration.

Here, we report MDP-presenting polymersomes (PS) utilized as artificial nanobacteria (NBA) to boost systemic NOD2 activation and the antitumor immune response. The surface of the PS is decorated with hydrophilic poly(ethylene glycol) (PEG) molecules, while the membrane comprises hydrophobic segment poly(trimethylene carbonate-*co*-dithiolane trimethylene carbonate) (P(TMC-DTC)). The dithiolane groups in the membrane participate in cross-linking during the self-assembly process, resulting in excellent stability in storage and in circulation while rapidly dissociating in the reducing environment inside cells.[29] The incorporation of doxorubicin (DOX) results in the initial liberation of tumor antigens through chemotherapy-induced immunogenic cell death (ICD). Subsequently, MDP-containing NBA facilitates the maturation of DCs and enhances antigen presentation while concurrently promoting the secretion of proinflammatory cytokines that are beneficial for T-cell activation. Furthermore, NBA facilitates the repolarization of M2 macrophages into M1 macrophages, synergistically inhibiting tumor growth in a B16-F10 melanoma model (Figure 1a). Moreover, NBA serves as carriers capable of delivering antigens to antigen-presenting cells, effectively reducing tumor development. These artificial nanobacteria represent a novel platform for cancer immunotherapy.

2. EXPERIMENTAL SECTION

2.1. Preparation and Characterization of NBA. To prepare NBA with a surface density of 38.5% MDP, a mixture consisting of 100 μL of poly(ethylene glycol)-*b*-poly(trimethylene carbonate-*co*-dithiolane trimethylene carbonate) (PEG-P(TMC-DTC) (2.2 kg/mol) and MDP-PEG-P(TMC-DTC) (2.5 kg/mol) at a 1:1 mass ratio (molar ratio, 9.1:8) in *N*,*N*-dimethylformamide (DMF, 40 mg/mL) was added to phosphate-buffered saline (PBS, pH 7.4, 10 mM, 900 μL) under stirring at 300 rpm. After stirring at room temperature (RT) for 10 min, the resulting dispersion was dialyzed against PBS (pH 7.4, 10 mM) for 6 h (MWCO 3 kDa) to remove DMF. The size distribution was measured by dynamic light scattering (DLS) and transmission electron microscopy (TEM). The theoretical surface density was calculated to

https://doi.org/10.1021/acsami.4c13041
ACS Appl. Mater. Interfaces 2024, 16, 61655−61663

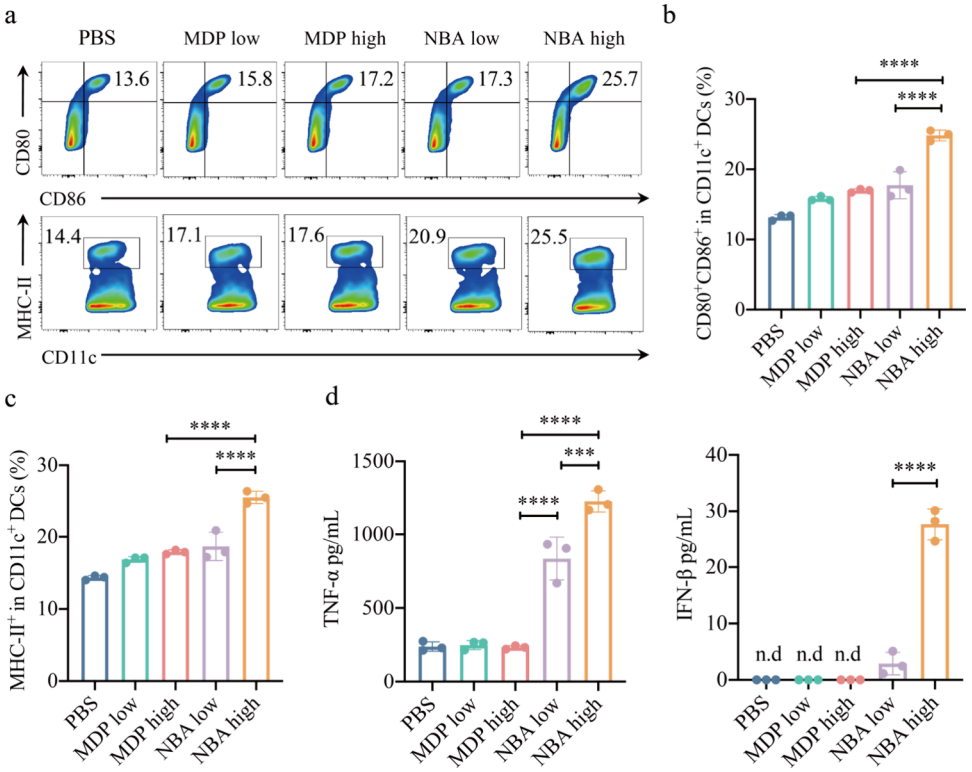

Figure 2. Immunostimulatory effects of NBA on BMDCs *in vitro*. (a) Representative flow cytometry plots. The maturation and antigen presentation of BMDCs promoted by PBS, free MDP, and NBA were analyzed via quantifications of (b) $CD80^+$ $CD86^+$ in $CD11c^+$ cells and (c) MHC-II^+ on BMDCs ($n = 3$). (d) Cytokines of TNF-α and IFN-β in the supernatant were measured by ELISA ($n = 3$), and n.d means not detected; p value: ***$p < 0.001$; ****$p < 0.0001$.

be 46.8%. As a blank control, we employed NBA with a surface density of 0% and subsequently evaluated the MDP concentration on the surface of this NBA by using the micro-BCA assay. The measured concentration of MDP was observed to be 82.3% of the theoretical concentration, leading to the conclusion that the actual surface density was estimated to be 38.5%.

2.2. Evaluation of RAW 264.7 Cell Activation by NBA. RAW 264.7 cells were cultured in six-well plates (1×10^6/well). After 12 h, the RAW 264.7 cells were respectively incubated with PBS, free MDP, or NBA (MDP, conc. 10 μg/mL, $n = 3$) at 37 °C with 5% CO_2. After 24 h, the culture medium was collected, and the concentrations of IL-1β and IL-6 were determined using ELISA kits. The mRNA expression of IL-1β, and IL-6 was determined using RT-PCR.

2.3. Evaluation of BMDC Activation by NBA. Immature bone marrow-derived dendritic cells (BMDCs) were cultured in 24-well plates (2×10^6/well). After 8 h, the BMDCs were incubated with PBS, free MDP at 1 μg/mL (low) or 10 μg/mL (high), and NBA at 1 μg MDP equiv/mL (low) or 10 μg MDP equiv/mL (high) at 37 °C with 5% CO_2 ($n = 3$). After 24 h, the cells were centrifuged and washed with FACS buffer (1% FBS in PBS), blocked with anti-mouse CD16/32 at RT, and then stained with CD11c-FITC, CD80-APC, CD86-PE, and I-A/I-E (MHC-II)-PerCP/Cy5.5 for 20 min at RT. The cells were then washed twice with FACS buffer and detected by flow cytometry. The culture medium was harvested for TNF-α and IFN-β ELISA assay.

2.4. Evaluation of the Antitumor Efficacy of NBA. C57BL/6 mice were inoculated subcutaneously with 2×10^5 B16-F10 cells in the right flank of each mouse on day −6 ($n = 8$) and randomly divided into PBS, NBA (1 mg MDP equiv/kg, i.v.), chemo (100 μg DOX per mouse, i.t.), chemo & MDP (combining DOX with free MDP, MDP 1 mg/kg, i.v.) and chemo & NBA groups. Three groups involving chemotherapy were administrated with chemotherapeutic drug at days 0, 3, and 6. MDP or NBA were treated on days 1, 4, 7, 10, and 13. Five mice were randomly selected to monitor tumor growth ($n = 5$), while the other three were used to analyze the serum cytokines and immune cells in tumor tissue ($n = 3$). DOX was delivered through encapsulation within PS that was formulated using PEG-P(TMC-DTC), achieving an actual drug loading content of 9.7%. Tumor growth was monitored every 3 days, and tumor volume was calculated by the following equation: tumor volume = length × $width^2 \times 0.5$. The serum concentrations of the proinflammatory cytokines TNF-α, IL-1β, and IL-6 on day 8 were determined using ELISA kits ($n = 3$).

2.5. Regulation of Immunosuppressed Tumor Microenvironment (TME) by NBA. Three mice of each treatment group were randomly selected and sacrificed on day 8. According to the protocol, single-cell suspensions of tumor tissue were prepared and lymphocytes were obtained by centrifugation after treatment with lymphocyte isolation solution.[30] Subsequently, the proportion of immune cells was analyzed using the isolated lymphocytes. Lymphocytes were blocked with anti-mouse CD16/32 at RT and stained with (i) CD11c-FITC, CD86-PE, and CD80-APC to analyze the DCs, (ii) CD11b-FITC, F4/80-PE, and CD206-APC to analyze the macrophages, and (iii) CD8-FITC, CD4-PE, and CD3-APC to analyze the infiltrating T-cells. The cells were then washed twice with FACS buffer and analyzed via flow cytometry.

2.6. Protective Effects of NBA@Ag. Tumor cell lysate acquisition and loading methods were consistent with our previous report.[31] C57BL/6 mice ($n = 3$) were immunized with PBS, PS@OVA (OVA, 1 mg/kg, s.c.) NBA@OVA (one vac, both MDP and OVA were 1 mg/kg, s.c.), NBA@OVA (two vac, s.c.), or Positive control (complete Freund's adjuvant, 100 μg per mouse, OVA 1 mg/kg, s.c.) on days 0 and 7. The serum concentration of OVA-IgG on days 7 and 14 was determined using an ELISA kit.

For the prophylactic study, C57BL/6 mice ($n = 3$) were immunized with PBS, PS@Ag (Ag from B16-F10 cell lysates, 1 mg/kg, s.c.) NBA@Ag (one vac, both MDP and Ag were 1 mg/kg, s.c.), or NBA@Ag (two vac) on days 0 and 7. Then, mice were subcutaneously inoculated with 2×10^5 B16-F10 cells in the right flank on day 14. Tumor growth was monitored every other day.

2.7. Statistical Analysis. All of the data are presented as the mean ± standard deviation (SD). Unless otherwise indicated, significant

https://doi.org/10.1021/acsami.4c13041
ACS Appl. Mater. Interfaces 2024, 16, 61655−61663

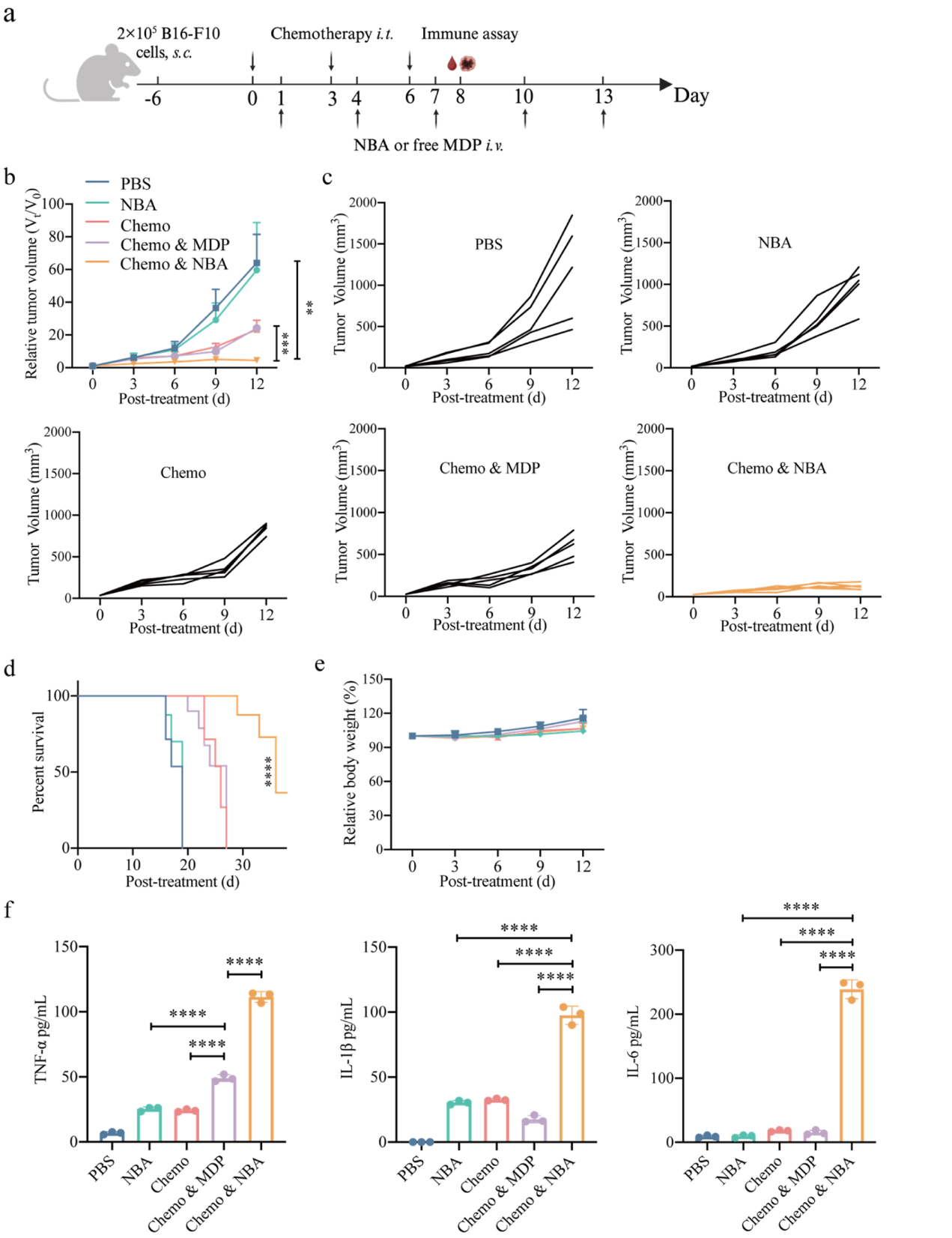

Figure 3. The NBA efficiently inhibits tumor growth and improves survival of tumor-bearing mice. (a) Timeline for experimental design to evaluate the *in vivo* therapeutic performance of NBA enhancing chemotherapy efficacy. C57BL/6 mice were inoculated subcutaneously with 2×10^5 B16-F10 cells in the right flank of each mouse on day −6 ($n = 8$) and randomly divided into PBS, NBA (i.v., 1 mg/kg), chemo (DOX loaded in PS with 9.7% content, 100 μg per mouse, i.t.), chemo & MDP (combining DOX with free MDP, MDP 1 mg/kg, i.v.) and chemo & NBA groups. (b−e) Five mice were randomly selected to monitor tumor growth ($n = 5$). (b) Relative tumor volume growth curve, (c) individual tumor growth curves, (d) survival curve of the treatment group, and (e) relative body weight curve. (f) The other three mice were used to analyze serum cytokines; serum concentrations of TNF-α, IL-1β, and IL-6 on day 8 were detected via ELISA ($n = 3$); p value: ** $p < 0.01$; *** $p < 0.001$; **** $p < 0.0001$.

https://doi.org/10.1021/acsami.4c13041
ACS Appl. Mater. Interfaces 2024, 16, 61655−61663

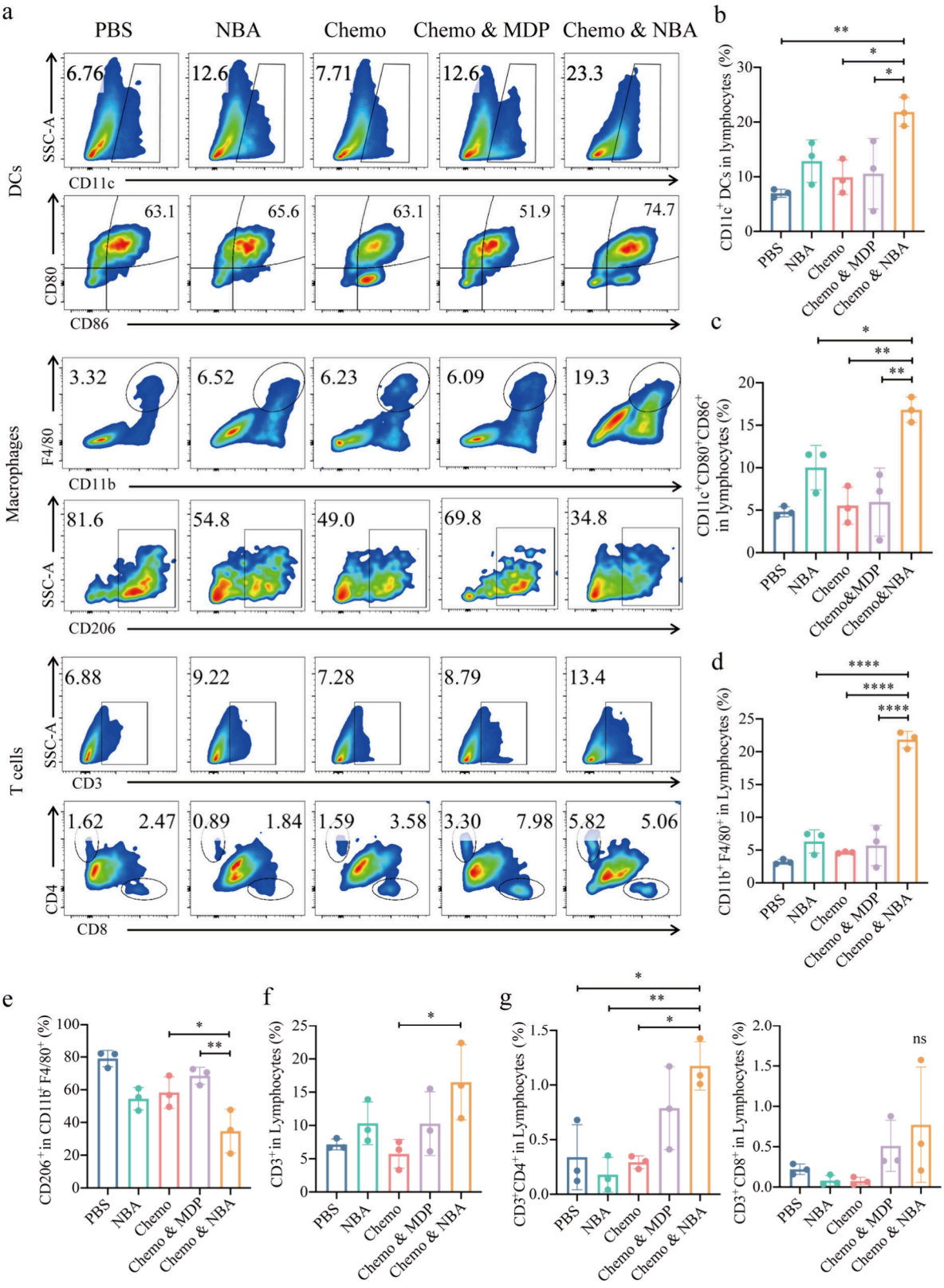

Figure 4. NBA reverses the immunosuppressive TME. Three mice were randomly selected from each group of the treatment experiment on day 8, and lymphocytes in tumor tissues were obtained using lymphocyte isolation solution and analyzed via flow cytometry ($n = 3$). (a) Representative flow cytometry plots and quantification of (b, c) DCs, (d, e) macrophages, and (f, g) T-cells; p value: $^{*}p < 0.05$; $^{**}p < 0.01$; $^{****}p < 0.0001$.

differences among groups were evaluated by one-way ANOVA with Tukey multiple comparison tests, and the survival rate was analyzed by the Kaplan−Meier method with a log-rank test for comparison using GraphPad Prism (version 8). p value: $^{*}p < 0.05$; $^{**}p < 0.01$; $^{***}p < 0.001$, and $^{****}p < 0.0001$.

https://doi.org/10.1021/acsami.4c13041
ACS Appl. Mater. Interfaces 2024, 16, 61655−61663

3. RESULTS AND DISCUSSION

3.1. Preparation of Artificial Nanobacteria. MDP-PEG-P(TMC-DTC) was synthesized according to our previous report,[15] and its structure was confirmed by ^{1}H NMR (Figures S1−S3). The NBA was fabricated through co-self-assembly of PEG-P(TMC-DTC) (M_n = 5.0−17 kg/mol) and MDP-functionalized PEG-P(TMC-DTC) (M_n = 7.5−17 kg/mol) at various ratios in PBS (pH 7.4, 10 mM), followed by dialysis (Figure 1a). To ensure the exposure of MDP on the outer surface, a longer PEG chain was utilized in MDP-PEG-P(TMC-DTC) compared to PEG-P(TMC-DTC). The surface density of MDP on NBA could be determined by micro-BCA assays with reference to the established standard curve. NBA with MDP densities ranging from 14.6% to 38.5% could be readily obtained. All NBA exhibited a small size of approximately 43 nm (Table S1, Figure S4a). Variations in the surface densities of MDP do not influence the stability of PS. This stability arises from the cross-linking of disulfide bonds within the DTC groups (Figure S4b,c), which has been thoroughly investigated in our prior reports.[32,33]

3.2. NBA Efficiently Stimulates Immune Cells. Given that MDP primarily stimulates the transduction of the NOD2 signaling pathway in monocytes, we evaluated the immunostimulatory effects of NBA on RAW 264.7 macrophages. Interestingly, Figure S5 shows that the endocytosis of NBA had a positive correlation with the surface density of MDP. The secretion of IL-6 and IL-1β is closely associated with the activation of the NOD2 pathway, which signifies the engagement of the NF-κB and MAPK signaling cascades that are downstream of NOD2.[16,34] As illustrated in Figure 1b,c, the modification of NBA with MDP on its surface resulted in an increased level of expression of these cytokines, evidencing a robust activation of the NOD2 pathways.

DCs serve as the primary APCs that play a crucial role in connecting innate and adaptive immune responses. We evaluated the effect of NBA on the maturation of BMDCs (Figure S6). The BMDCs were treated with either free MDP or NBA for 24 h. Two concentrations of MDP, 1 μg/mL (low) and 10 μg/mL (high), were utilized in the study. The results revealed that both concentrations of free MDP were capable of activating BMDCs to a certain extent (Figure 2a,b). Notably, treatment with NBA at a concentration equivalent to 10 μg MDP/mL significantly upregulated the expression of the costimulatory molecules CD80 and CD86, indicating a stimulatory effect of NBA on BMDC maturation. Such treatment also resulted in a 1.6-fold increase in the expression of major histocompatibility complex class II (MHC-II) molecules (Figure 2c). Furthermore, in sharp contrast to free MDP, NBA induced the notable secretion of inflammatory cytokines from BMDCs. Treatment with NBA at concentrations equivalent to 1 and 10 μg MDP/mL led to significant increases in tumor necrosis factor alpha (TNF-α) levels, compared to controls treated with free MDP or phosphate-buffered saline (PBS) (Figure 2d). Given the bacterial origin of MDP, the ability of MDP to induce an anti-infection response was assessed by measuring interferon-β (IFN-β) secretion. NBA treatment significantly enhanced IFN-β secretion compared with minimal IFN-β release observed with free MDP. The findings suggest that NBA amplifies the proinflammatory effects of MDP in DCs by boosting the innate immune response. The production of cytokines stimulated by MDP and NBA in RAW 264.7 cells and BMDCs is illustrated in Table S2. Given that NBA exhibiting a higher MDP density demonstrates enhanced uptake and activation of BMDCs, subsequent experiments, unless stated otherwise, utilized NBA with an MDP density of 38.5%.

3.3. NBA Enhances Chemo-Immunotherapy. Enhancing the release of tumor antigens and improving the efficiency of antigen presentation by APCs are essential for the development of safe and effective *in situ* tumor vaccines.[35] DOX could induce ICD, which leads to the release of tumor-associated antigens and the initiation of antitumor immunity.[36−38] Here, we investigated the potential of NBA to enhance the chemo-immunotherapy of malignant murine melanoma in combination with DOX. B16-F10-bearing mice were treated with PBS, NBA, DOX (chemo), the combination of DOX and free MDP (chemo & MDP), and the combination of DOX and NBA (chemo & NBA), respectively. DOX was encapsulated in PS formed by PEG-P(TMC-DTC) with a 9.7% loading content[39] and administrated intratumorally at a dose of 100 μg DOX per mouse on days 0, 3, and 6, while NBA and free MDP were intravenously injected at a dose of 1 mg MDP equiv/kg on days 1, 4, 7, 10, and 13 (Figure 3a). DOX was given 1 day earlier than NBA to generate ICD and amplify immune response. The results demonstrated that NBA alone exhibited minimal antitumor activity, and the addition of free MDP did not enhance the efficacy of chemotherapy (Figure 3b,c). In contrast, NBA significantly augmented the antitumor performance of DOX. Consequently, the chemo & NBA group significantly prolonged the survival of tumor-bearing mice compared to the chemo and chemo & MDP groups (Figure 3d). All treatment regimens led to negligible variations in body weight (Figure 3e). The NBA exhibited no significant cytotoxic effects on normal cells (Figure S7). Furthermore, throughout the entire *in vivo* experiment, no adverse effects were noted in the mice, including lethargy or alterations in posture, indicating that NBA containing a high density of MDP does not induce obvious inflammatory side effects. Analysis of cytokines in plasma on day 8 showed that the chemo & NBA group significantly elevated the secretion of TNF-α, IL-1β, and IL-6 compared to all control groups (Figure 3f). These findings collectively indicate that NBA substantially enhances the therapeutic efficacy of chemotherapy.

3.4. NBA Reverses the Immunosuppressive Tumor Microenvironment. The immunosuppressive tumor microenvironment (TME), characterized by a scarcity of proinflammatory immune cell infiltration and a high prevalence of suppressive immune cells, plays a significant role in fostering drug resistance and immune escape.[40] Therefore, the status of tumor-infiltrating immune cells was investigated (Figure S8). The combination treatment of chemo & NBA led to a 2.2-fold increase in DC infiltration and a 3.0-fold increase in the proportion of mature DCs within the tumor tissue compared to the chemo group (Figure 4a−c). Tumor-associated macrophages (TAMs), often identified as M2-type macrophages, actively support tumor growth while inhibiting cytotoxic T-cell responses.[41] Notably, NBA intervention led to a 1.7-fold reduction in the population of M2-type macrophages in comparison to chemotherapy alone (Figure 4d,e). Furthermore, the combination therapy of chemo & NBA also triggered a significant increase in tumor-infiltrating T-cells including $CD8^+$ effector T-cells and $CD4^+$ T helper cells (Figure 4f,g), demonstrating that NBA enhanced the systemic immune response and reversed the immunosuppressive TME. The antitumor mechanism of chemo & NBA involves tumor reduction and ICD induction by chemo to facilitate the release

https://doi.org/10.1021/acsami.4c13041
ACS Appl. Mater. Interfaces 2024, 16, 61655−61663

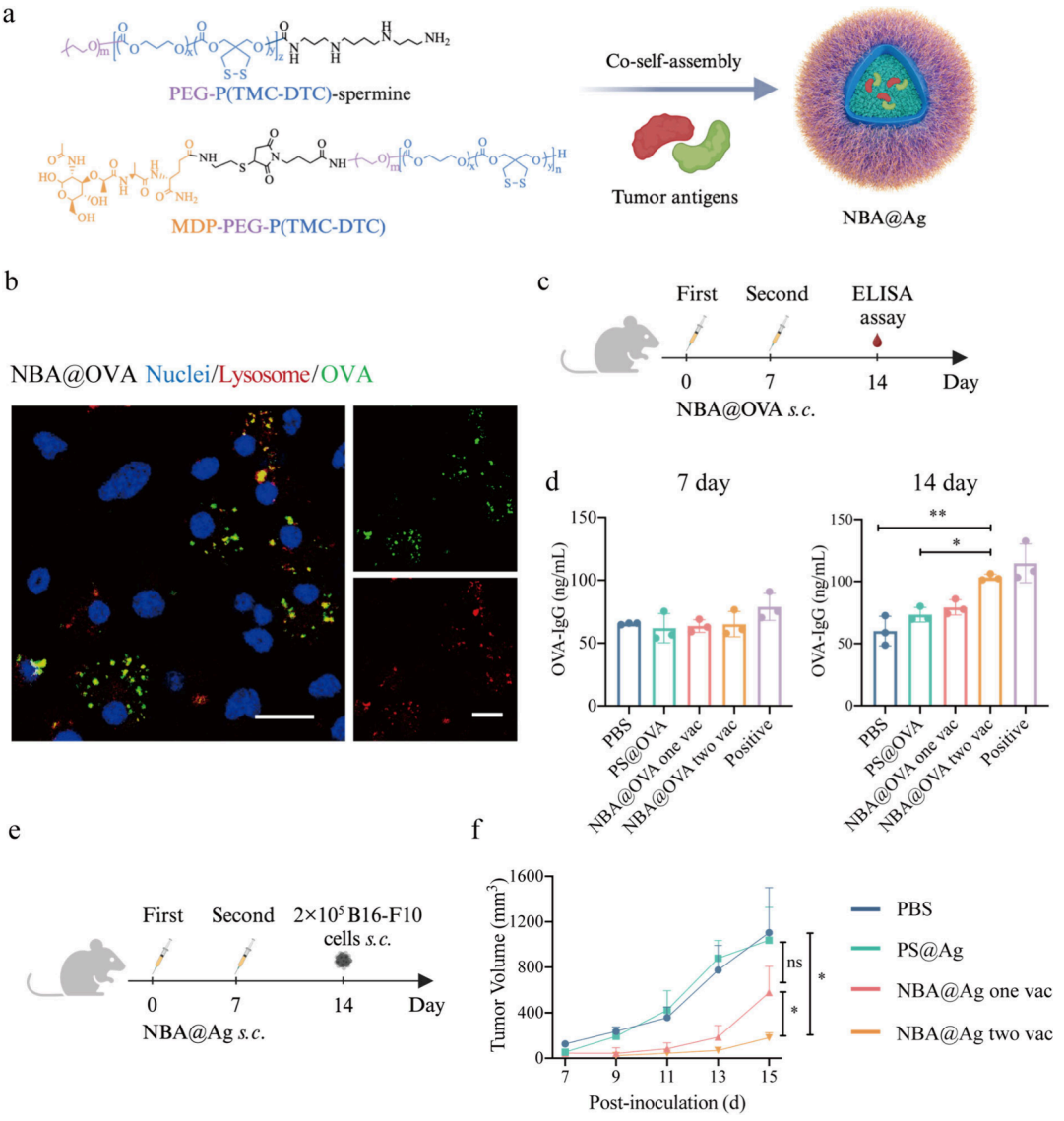

Figure 5. NBA@Ag serves as a prophylactic tumor vaccine to protect the tumor from progressing. (a) Schematic illustration of NBA encapsulating Ag to form NBA@Ag. (b) CLSM image illustrating the delivery of antigens by NBA@OVA to BMDCs. Scale bar: 20 μm. (c) Timeline for NBA@OVA inducing OVA-IgG production *in vivo*. C57BL/6 mice ($n = 3$) were immunized with PBS, PS@OVA (OVA, 1 mg/kg, s.c.), NBA@OVA (one vac, both MDP and OVA were 1 mg/kg, s.c.), NBA@OVA (two vac, s.c.), and Positive control (complete Freund's adjuvant, 100 μg per mouse, 1 mg/kg, s.c.) on days 0 and 7. Serum was obtained for ELISA assay at days 7 and 14. (d) Serum concentration of OVA-IgG on days 7 and 14. (e) Timeline for NBA@Ag preventing melanoma model growth. C57BL/6 mice ($n = 3$) were immunized with PBS, PS@Ag (Ag from B16-F10 cell lysates, 1 mg/kg, s.c.), NBA@Ag (one vac, both MDP and Ag were 1 mg/kg, s.c.), and NBA@Ag (two vac, s.c.) on days 0 and 7, then inoculated subcutaneously with 2×10^5 B16-F10 cells in the right flank of each mouse on day 14. (f) The tumor volume curve was monitored; p value: $^*p < 0.05$; $^{**}p < 0.01$.

of tumor antigens and activation of APCs by NBA, thereby eliciting a specific antitumor immune response.

3.5. NBA Encapsulating Antigens as Prophylactic Tumor Vaccines. We further investigated whether NBA could also be employed to formulate prophylactic tumor vaccines to augment the presentation of tumor antigens by DCs. Utilizing the charge interaction of spermine-functionalized PEG-P(TMC-DTC), the antigen was encapsulated within the internal cavity of NBA to form an NBA@Ag tumor vaccine (Figure 5a). The lysate or antigen could be entirely encapsulated within the aqueous core of NBA at a drug loading content of 1%, resulting in NBA@Ag with a size of 58 nm, consistent with our prior studies.[15,29,31] The DTC engages in a reversible cross-linking reaction during the assembly process. This cross-linking will be quickly dissociated in the reducing environment of the cytoplasm, consequently facilitating the release of the encapsulated lysate or antigens.[31] Figure 5b shows that antigens could be efficiently delivered into BMDCs by NBA. Given the well-documented anti-infective immune response elicited by MDP, we initially assessed the ability of NBA@Ag to induce an antibody response *in vivo*. The model antigen OVA was loaded into NBA and injected subcutaneously at the tail base on days 0 and 7, and the serum levels of OVA-IgG were analyzed on days 7 and 14 (Figure 5c). Immunization resulted in a significant elevation in the OVA-IgG antibody level, comparable to those seen in the Positive control group (Figure 5d). Tumor cell lysates are derived from whole tumor cells that contain abundant tumor-specific antigens (TSAs), allowing induction of a broad antitumor immunity to minimize cancer immune escape caused by tumor heterogeneity. Subsequently, tumor cell lysates were

https://doi.org/10.1021/acsami.4c13041
ACS Appl. Mater. Interfaces 2024, 16, 61655−61663

incorporated into NBA using a previously reported method,[31] and mice were immunized subcutaneously at the tail base before being challenged with B16-F10 cells (Figure 5e). Remarkably, NBA@Ag exhibited a pronounced inhibition of tumor growth, with two immunizations demonstrating a stronger preventive effect compared to a single immunization (Figure 5f).

4. CONCLUSION

In conclusion, the artificial NBA that we have developed has proven effective in augmenting MDP utilization for NOD2 stimulation. NBA has demonstrated the ability to significantly increase the expression of proinflammatory genes and the secretion of cytokines associated with innate immunity. Moreover, NBA has shown promise in promoting the maturation of DCs and facilitating antigen presentation, thereby enhancing the adaptive immune response. When employed in the context of antitumor therapy, NBA enhances the therapeutic effect of chemotherapy and remodels the immunosuppressive TME. Additionally, NBA loaded with tumor antigens has exhibited prophylactic effects against tumorigenesis. The artificial nanobacteria present themselves as a potent systemic immunoadjuvant for activating NOD2 systemically and hold significant potential for the field of cancer immunotherapy.

■ ASSOCIATED CONTENT

Supporting Information

The Supporting Information is available free of charge at https://pubs.acs.org/doi/10.1021/acsami.4c13041.

Additional text with details on the experimental section and additional experimental results (PDF)

■ AUTHOR INFORMATION

Corresponding Author

Zhiyuan Zhong − *Biomedical Polymers Laboratory, College of Chemistry, Chemical Engineering and Materials Science, and State Key Laboratory of Radiation Medicine and Protection and College of Pharmaceutical Sciences, Soochow University, Suzhou 215123, P.R. China;* orcid.org/0000-0003-4175-4741; Phone: +86-512-65880098; Email: zyzhong@suda.edu.cn

Authors

Guanhong Cui − *Biomedical Polymers Laboratory, College of Chemistry, Chemical Engineering and Materials Science, and State Key Laboratory of Radiation Medicine and Protection, Soochow University, Suzhou 215123, P.R. China*

Yinping Sun − *Biomedical Polymers Laboratory, College of Chemistry, Chemical Engineering and Materials Science, and State Key Laboratory of Radiation Medicine and Protection, Soochow University, Suzhou 215123, P.R. China*

Shenqiang Wang − *College of Pharmaceutical Sciences, Soochow University, Suzhou 215123, P.R. China*

Fenghua Meng − *Biomedical Polymers Laboratory, College of Chemistry, Chemical Engineering and Materials Science, and State Key Laboratory of Radiation Medicine and Protection, Soochow University, Suzhou 215123, P.R. China;* orcid.org/0000-0002-8608-7738

Complete contact information is available at: https://pubs.acs.org/10.1021/acsami.4c13041

Author Contributions

Z.Z. and G.C. conceived and designed the experiments. G.C. and Y.S. performed the experiments. G.C. and S.W. analyzed and processed the data. F.M. provided advice in designing and conducting experiments. All authors participated the discussion of the results and made comments to the manuscript. G.C. wrote the initial manuscript. Z.Z., S.W., and G.C. further revised the manuscript.

Notes

The authors declare no competing financial interest.

■ ACKNOWLEDGMENTS

This work was financially supported by the National Key R&D Program of China (2021YFB3800900) and the National Natural Science Foundation of China (52233007).

■ REFERENCES

(1) Lin, M. J.; Svensson-Arvelund, J.; Lubitz, G. S.; Marabelle, A.; Melero, I.; Brown, B. D.; Brody, J. D. Cancer vaccines: the next immunotherapy frontier. *Nat. Cancer* **2022**, *3*, 911−926.

(2) Saxena, M.; van der Burg, S. H.; Melief, C. J. M.; Bhardwaj, N. Therapeutic cancer vaccines. *Nat. Rev. Cancer* **2021**, *21*, 360−378.

(3) Walsh, K. P.; Mills, K. H. G. Dendritic cells and other innate determinants of T helper cell polarisation. *Trends Immunol.* **2013**, *34*, 521−530.

(4) Zhao, T.; Cai, Y.; Jiang, Y.; He, X.; Wei, Y.; Yu, Y.; Tian, X. Vaccine adjuvants: mechanisms and platforms. *Signal Transduct. Target. Ther.* **2023**, *8*, 283.

(5) Banstola, A.; Jeong, J.-H.; Yook, S. Immunoadjuvants for cancer immunotherapy: A review of recent developments. *Acta Biomater.* **2020**, *114*, 16−30.

(6) Kuai, R.; Ochyl, L. J.; Bahjat, K. S.; Schwendeman, A.; Moon, J. J. Designer vaccine nanodiscs for personalized cancer immunotherapy. *Nat. Mater.* **2017**, *16*, 489−496.

(7) Liu, S. L.; Jiang, Q.; Zhao, X.; Zhao, R. F.; Wang, Y. N.; Wang, Y. M.; Liu, J. B.; Shang, Y. X.; Zhao, S.; Wu, T. T.; Zhang, Y. L.; Nie, G. J.; Ding, B. Q. A DNA nanodevice-based vaccine for cancer immunotherapy. *Nat. Mater.* **2021**, *20*, 431−433.

(8) Wang, X.; Liu, Y. Q.; Xue, C. C.; Hu, Y.; Zhao, Y. Y.; Cai, K. Y.; Li, M. H.; Luo, Z. A protein-based cGAS-STING nanoagonist enhances T cell-mediated anti-tumor immune responses. *Nat. Commun.* **2022**, *13*, 5685.

(9) Stephen, J.; Scales, H. E.; Benson, R. A.; Erben, D.; Garside, P.; Brewer, J. M. Neutrophil swarming and extracellular trap formation play a significant role in Alum adjuvant activity. *npj Vaccines* **2017**, *2*, 1.

(10) Datoo, M. S.; Natama, M. H.; Somé, A.; Traoré, O.; Rouamba, T.; Bellamy, D.; Yameogo, P.; Valia, D.; Tegneri, M.; Ouedraogo, F.; Soma, R.; Sawadogo, S.; Sorgho, F.; Derra, K.; Rouamba, E.; Orindi, B.; Ramos Lopez, F.; Flaxman, A.; Cappuccini, F.; Kailath, R.; Elias, S.; Mukhopadhyay, E.; Noe, A.; Cairns, M.; Lawrie, A.; Roberts, R.; Valéa, I.; Sorgho, H.; Williams, N.; Glenn, G.; Fries, L.; Reimer, J.; Ewer, K. J.; Shaligram, U.; Hill, A. V. S.; Tinto, H. Efficacy of a low-dose candidate malaria vaccine, R21 in adjuvant Matrix-M, with seasonal administration to children in Burkina Faso: a randomised controlled trial. *Lancet* **2021**, *397*, 1809−1818.

(11) Verma, S. K.; Mahajan, P.; Singh, N. K.; Gupta, A.; Aggarwal, R.; Rappuoli, R.; Johri, A. K. New-age vaccine adjuvants, their development, and future perspective. *Front. Immunol.* **2023**, *14*, 1043109.

(12) Guzelj, S.; Nabergoj, S.; Gobec, M.; Pajk, S.; Klančič, V.; Slütter, B.; Frkanec, R.; Štimac, A.; Šket, P.; Plavec, J.; Mlinarič-Raščan, I.; Jakopin, Ž. Structural Fine-Tuning of Desmuramylpeptide NOD2 Agonists Defines Their In Vivo Adjuvant Activity. *J. Med. Chem.* **2021**, *64*, 7809−7838.

(13) Stafford, C. A.; Gassauer, A.-M.; de Oliveira Mann, C. C.; Tanzer, M. C.; Fessler, E.; Wefers, B.; Nagl, D.; Kuut, G.; Sulek, K.; Vasilopoulou, C.; Schwojer, S. J.; Wiest, A.; Pfautsch, M. K.; Wurst, W.; Yabal, M.; Fröhlich, T.; Mann, M.; Gisch, N.; Jae, L. T.; Hornung,

V. Phosphorylation of muramyl peptides by NAGK is required for NOD2 activation. *Nature* **2022**, *609*, 590−596.
(14) Geddes, K.; Magalhães, J. G.; Girardin, S. E. Unleashing the therapeutic potential of NOD-like receptors. *Nat. Rev. Drug Discov.* **2009**, *8*, 465−479.
(15) Zhang, P.; Wang, T.; Cui, G.; Ye, R.; Wan, W.; Liu, T.; Zheng, Y.; Zhong, Z. Systemic Multifunctional Nanovaccines for Potent Personalized Immunotherapy of Acute Myeloid Leukemia. *Adv. Mater.* **2024**, *36*, No. 2407189.
(16) Hu, C.; Sun, L.; Hu, Y.; Lu, D.; Wang, H.; Tang, S. Functional characterization of the NF-κB binding site in the human NOD2 promoter. *Cell. Mol. Immunol.* **2010**, *7*, 288−295.
(17) Caruso, R.; Warner, N.; Inohara, N.; Núñez, G. NOD1 and NOD2: Signaling, Host Defense, and Inflammatory Disease. *Immunity* **2014**, *41*, 898−908.
(18) Dong, Y.; Wang, S.; Wang, C.; Li, Z.; Ma, Y.; Liu, G. Antagonizing NOD2 Signaling with Conjugates of Paclitaxel and Muramyl Dipeptide Derivatives Sensitizes Paclitaxel Therapy and Significantly Prevents Tumor Metastasis. *J. Med. Chem.* **2017**, *60*, 1219−1224.
(19) Wen, X.; Zheng, P.; Ma, Y.; Ou, Y.; Huang, W.; Li, S.; Liu, S.; Zhang, X.; Wang, Z.; Zhang, Q.; Cheng, W.; Lin, R.; Li, H.; Cai, Y.; Hu, C.; Wu, N.; Wan, L.; Pan, T.; Rao, J.; Bei, X.; Wu, W.; Jin, J.; Yan, J.; Liu, G. Salutaxel, a Conjugate of Docetaxel and a Muramyl Dipeptide (MDP) Analogue, Acts as Multifunctional Prodrug That Inhibits Tumor Growth and Metastasis. *J. Med. Chem.* **2018**, *61*, 1519−1540.
(20) Tacyildiz, N.; Unal, E.; Dincaslan, H.; Cakmak, H. M.; Kose, K.; Tanyildiz, G.; Kartal, O. Muramyl Tripeptide Plus Chemotherapy Reduces Metastasis in Non-Metastatic Osteosarcoma: A Single-Center Experience. *Asian Pac. J. Cancer Prev.* **2020**, *21*, 715−720.
(21) Kamboj, A.; Patil, M. T.; Petrovsky, N.; Salunke, D. B. Structure-activity relationship in NOD2 agonistic muramyl dipeptides. *Eur. J. Med. Chem.* **2024**, *271*, No. 116439.
(22) Iwicka, E.; Hajtuch, J.; Dzierzbicka, K.; Inkielewicz-Stepniak, I. Muramyl dipeptide-based analogs as potential anticancer compounds: Strategies to improve selectivity, biocompatibility, and efficiency. *Front. Oncol.* **2022**, *12*, No. 970967.
(23) Guimarães, D.; Cavaco-Paulo, A.; Nogueira, E. Design of liposomes as drug delivery system for therapeutic applications. *Int. J. Pharm.* **2021**, *601*, No. 120571.
(24) Martel, A. L.; Fraleigh, N. L.; Picard, E.; Lewicky, J. D.; Pawelec, G.; Lee, H.; Ma, G. W.; Mousavifar, L.; Roy, R.; Le, H.-T. Novel immunomodulatory properties of low dose cytarabine entrapped in a mannosylated cationic liposome. *Int. J. Pharm.* **2021**, *606*, No. 120849.
(25) Knotigova, P. T.; Zyka, D.; Masek, J.; Kovalova, A.; Krupka, M.; Bartheldyova, E.; Kulich, P.; Koudelka, S.; Lukac, R.; Kauerova, Z.; Vacek, A.; Horynova, M. S.; Kozubik, A.; Miller, A. D.; Fekete, L.; Kratochvilova, I.; Jezek, J.; Ledvina, M.; Raska, M.; Turanek, J. Molecular Adjuvants Based on Nonpyrogenic Lipophilic Derivatives of norAbuMDP/GMDP Formulated in Nanoliposomes: Stimulation of Innate and Adaptive Immunity. *Pharm. Res.* **2015**, *32*, 1186−1199.
(26) Mori, K.; Ando, K.; Heymann, D. Liposomal muramyl tripeptide phosphatidyl ethanolamine: a safe and effective agent against osteosarcoma pulmonary metastases. *Expert Rev. Anticancer Ther* **2008**, *8*, 151−159.
(27) Olusanya, T. O. B.; Haj Ahmad, R. R.; Ibegbu, D. M.; Smith, J. R.; Elkordy, A. A. Liposomal Drug Delivery Systems and Anticancer Drugs. *Molecules* **2018**, *23*, 907.
(28) Briuglia, M.-L.; Rotella, C.; McFarlane, A.; Lamprou, D. A. Influence of cholesterol on liposome stability and on in vitro drug release. *Drug Deliv. Transl. Res.* **2015**, *5*, 231−242.
(29) Qu, L.; Cui, G.; Sun, Y.; Ye, R.; Sun, Y.; Meng, F.; Wang, S.; Zhong, Z. A Biomimetic Autophagosomes-Based Nanovaccine Boosts Anticancer Immunity. *Adv. Mater.* **2024**, *36*, No. 2409590.
(30) Tan, Y. S.; Lei, Y. L. Isolation of Tumor-Infiltrating Lymphocytes by Ficoll-Paque Density Gradient Centrifugation. *Methods Mol. Biol.* **2019**, *1960*, 93−99.
(31) Cui, G.; Sun, Y.; Qu, L.; Shen, C.; Sun, Y.; Meng, F.; Zheng, Y.; Zhong, Z. Uplifting Antitumor Immunotherapy with Lymph-Node-Targeted and Ratio-Controlled Codelivery of Tumor Cell Lysate and Adjuvant. *Adv. Healthc. Mater.* **2024**, *13*, 2303690.
(32) Zhang, Y.; Yue, S.; Haag, R.; Sun, H.; Zhong, Z. An intelligent cell-selective polymersome-DM1 nanotoxin toward triple negative breast cancer. *J. Controlled Release* **2021**, *340*, 331−341.
(33) Du, J.; Yue, S.; Li, C.; Li, J.; Zhao, S.; Dong, Y.; Zhang, Y.; Cheng, R.; Sun, H.; Zhong, Z. Exogenous CD38 upregulation enables high-efficacy dually cascade targeted molecular therapy of leukemia. *Nano Today* **2023**, *50*, No. 101872.
(34) Hedl, M.; Abraham, C. Nod2-Induced Autocrine Interleukin-1 Alters Signaling by ERK and p38 to Differentially Regulate Secretion of Inflammatory Cytokines. *Gastroenterology* **2012**, *143*, 1530−1543.
(35) Gong, N.; Alameh, M.-G.; El-Mayta, R.; Xue, L.; Weissman, D.; Mitchell, M. J. Enhancing in situ cancer vaccines using delivery technologies. *Nat. Rev. Drug Discov.* **2024**, *23*, 607−625.
(36) Zhang, J.; Sun, X.; Zhao, X.; Yang, C.; Shi, M.; Zhang, B.; Hu, H.; Qiao, M.; Chen, D.; Zhao, X. Combining immune checkpoint blockade with ATP-based immunogenic cell death amplifier for cancer chemo-immunotherapy. *Acta Pharm. Sin. B* **2022**, *12*, 3694−3709.
(37) Xu, Y.; Guo, Y.; Zhang, C.; Zhan, M.; Jia, L.; Song, S.; Jiang, C.; Shen, M.; Shi, X. Fibronectin-Coated Metal-Phenolic Networks for Cooperative Tumor Chemo-/Chemodynamic/Immune Therapy via Enhanced Ferroptosis-Mediated Immunogenic Cell Death. *ACS Nano* **2022**, *16*, 984−996.
(38) Yu, Z.; Guo, J.; Hu, M.; Gao, Y.; Huang, L. Icaritin Exacerbates Mitophagy and Synergizes with Doxorubicin to Induce Immunogenic Cell Death in Hepatocellular Carcinoma. *ACS Nano* **2020**, *14*, 4816−4828.
(39) Zou, Y.; Wei, J.; Xia, Y.; Meng, F.; Yuan, J.; Zhong, Z. Targeted chemotherapy for subcutaneous and orthotopic non-small cell lung tumors with cyclic RGD-functionalized and disulfide-crosslinked polymersomal doxorubicin. *Signal Transduct. Target. Ther.* **2018**, *3*, 32.
(40) Baharom, F.; Ramirez-Valdez, R. A.; Khalilnezhad, A.; Khalilnezhad, S.; Dillon, M.; Hermans, D.; Fussell, S.; Tobin, K. K. S.; Dutertre, C.-A.; Lynn, G. M.; Müller, S.; Ginhoux, F.; Ishizuka, A. S.; Seder, R. A. Systemic vaccination induces CD8+ T cells and remodels the tumor microenvironment. *Cell* **2022**, *185*, 4317.
(41) Chen, Y.; Gong, L.; Cao, Y.; Liu, Z.; Wang, Y.; Cheng, H.; Feng, Y.; Yao, S.; Yin, Y.; Wu, Z.; Huang, Z. Reprogramming tumor-associated macrophages by a dually targeted milk exosome system as a potent monotherapy for cancer. *J. Controlled Release* **2024**, *366*, 395−409.

https://doi.org/10.1021/acsami.4c13041
ACS Appl. Mater. Interfaces 2024, 16, 61655−61663